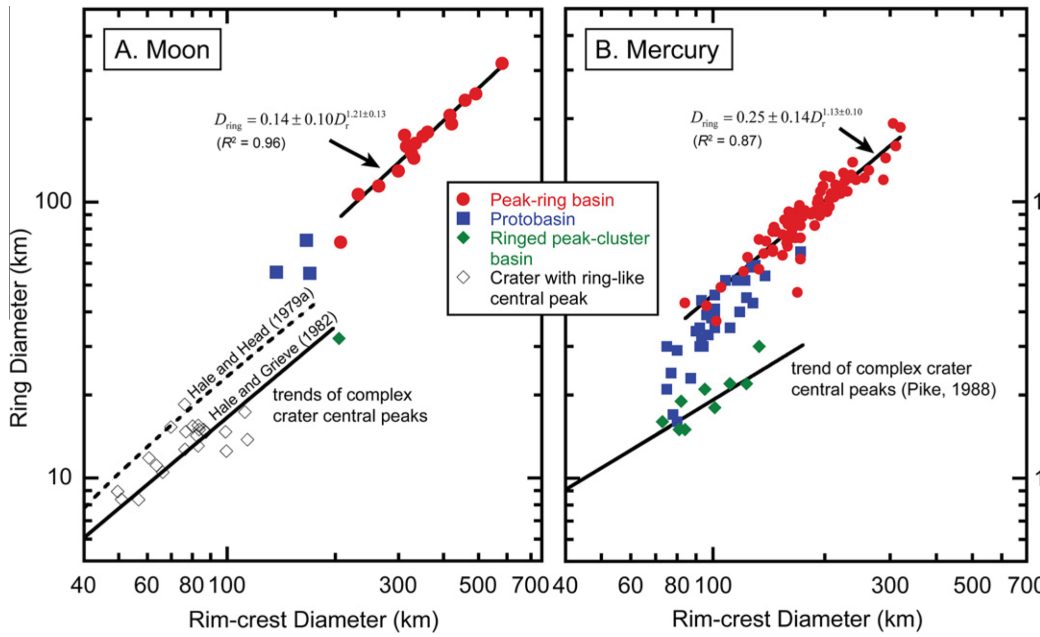

Fig. 4. Log–log plots of ring diameter (D_{ring}) versus rim-crest diameter (D_r) for peak-ring basins (red circles), protobasins (blue squares), and ringed peak-cluster basins (green diamonds) on the Moon (A, Tables A1–A3) and Mercury (B, from Baker et al., 2011). Also plotted for the Moon are the ring and rim-crest diameters for craters exhibiting ring-like central peaks (Table A3). Peak-ring basins follow a power law trend of $D_{ring} = 0.14 \pm 0.10(D_r)^{1.21\pm0.13}$ (R^2 = 0.96) on the Moon, which is very similar to the power law trend for peak-ring basins on Mercury [$D_{ring} = 0.25 \pm 0.14(D_r)^{1.13\pm0.10}$, R^2 = 0.87, Baker et al., 2011) (Table 2). Protobasins occur at smaller diameters, but appear to follow the tail-end of the peak-ring basin trend for the Moon and Mercury. Also shown are the trends for the diameters of central peaks (D_{cp}) in complex craters on the Moon ($D_{cp} = 0.259D_r - 2.57$, Hale and Head, 1979a, and $D_{cp} = 0.107(D_r)^{1.095}$, Hale and Grieve, 1982) and Mercury ($D_{cp} = 0.44(D_r)^{0.82}$, Pike, 1988). The ringed peak-cluster basin, Humboldt, and craters with ring-like central peaks plot at intermediate values between the two complex crater trends for the Moon. (For interpretation of the references to color in this figure legend, the reader is referred to the web version of this article.)

populations can now be cataloged based on complete, or nearly complete, data coverage of the planetary surface, we can be confident that we are using populations rather than samples of particular crater and basin morphologies when calculating onset diameters. While the use of the 5th percentile to define peak-ring basin onset diameter does not rely on more than a single basin population and is not directly derived from the observed morphological transition between complex crater and peak-ring basin, peak-ring basin onset diameters calculated by this method consistently fall within the uncertainties of onset diameters calculated using a method based on the diameters of overlapping morphologies, as described above (Table 1).

6. Analysis and interplanetary comparisons

Our refined catalog of transitional lunar basin types between complex craters and multi-ring basins permits us to better compare and evaluate several key characteristics of basin populations on the Moon and the terrestrial planets. These characteristics include: (1) ring and rim-crest diameter systematics, (2) surface density of peak-ring basins, and (3) peak-ring basin onset diameter. The airless body, Mercury, has the largest population of preserved peak-ring basins and protobasins in the inner Solar System (Baker et al., 2011), and thus provides an important dataset for comparison with the population of peak-ring basins and protobasins on the Moon. The basin catalogs for Venus and Mars should also be considered in interplanetary comparisons; however, resurfacing, erosion, and the effects of volatiles have influenced the present populations and morphologies of basins on these planets, rendering them less useful in comparison studies. Since the impact record on Earth is largely incomplete and highly modified by erosion, interior structures cannot be accurately identified and therefore present large uncertainties when used in interplanetary comparisons. As such, impact structures on Earth are not used in this study. In the following sections, we analyze our new catalog of basins on the Moon and identify key similarities and differences with the other planetary bodies, especially Mercury. In the next section, these comparisons are then placed in context of the predictions of a model of peak-ring basin formation that explains their morphological characteristics as resulting from the nonlinear scaling of impact melt.

6.1. Ring versus rim-crest diameter trends

Following the methods of Pike (1988) and Baker et al. (2011), we plot the ring diameter versus the rim-crest diameter in log–log space for lunar peak-ring basins, protobasins, and craters with ring-like central peaks and the ringed peak-cluster basin, Humboldt. Several trends are observed. First, peak-ring basins form a straight-line in log–log space at large rim-crest diameters in Fig. 4, and can be fit by a power law trend of the form

$$D_{ring} = AD_r^p \quad (1)$$

where D_{ring} is the diameter of the interior ring, D_r is the basin rim-crest diameter, and p is the slope of the best-fitting line on a log–log plot. Power-law fits were calculated in KaleidaGraph (Synergy Software, www.synergy.com), which uses the Levenberg–Marquardt non-linear curve-fitting algorithm (Press et al., 1992) to iteratively minimize the sum of the squared errors in the ordinate. The use of this criterion for minimization implies that fractional errors in the estimates of interior ring diameters are regarded as larger than those for estimates of the rim-crest diameter.

We calculate a power law fit of $D_{ring} = 0.14 \pm 0.10(D_r)^{1.21\pm0.13}$ (R^2 = 0.96, where R is the correlation coefficient for the given dataset on a log–log plot) for lunar peak-ring basins (Table 2). This fit is very similar to a power law fit to peak-ring basins on Mercury